Neuron, Vol. 36, 649–659, November 14, 2002, Copyright ©2002 by Cell Press

Depolarization Redistributes Synaptic Membrane and Creates a Gradient of Vesicles on the Synaptic Body at a Ribbon Synapse

David Lenzi,[1,4] John Crum,[2] Mark H. Ellisman,[2] and William M. Roberts[1,3]
[1]Institute of Neuroscience
University of Oregon
Eugene, Oregon 97403
[2]National Center for Microscopy and Imaging Research and
Department of Neurosciences
University of California, San Diego
La Jolla, California 92093

Summary

We used electron tomography of frog saccular hair cells to reconstruct presynaptic ultrastructure at synapses specialized for sustained transmitter release. Synaptic vesicles at inhibited synapses were abundant in the cytoplasm and covered the synaptic body at high density. Continuous maximal stimulation depleted 73% of the vesicles within 800 nm of the synapse, with a concomitant increase in surface area of intracellular cisterns and plasmalemmal infoldings. Docked vesicles were depleted 60%–80% regardless of their distance from the active zone. Vesicles on the synaptic body were depleted primarily in the hemisphere facing the plasmalemma, creating a gradient of vesicles on its surface. We conclude that formation of new synaptic vesicles from cisterns is rate limiting in the vesicle cycle.

Introduction

Ribbon-class synapses are found in sensory cells in the vertebrate eye and ear, and in certain other nonspiking neurons specialized for tonic synaptic transmission (Jusola et al., 1996). They are distinguished by a prominent presynaptic organelle, the synaptic ribbon, and its shell of tethered synaptic vesicles (Wagner, 1997; Lenzi and von Gersdorff, 2001). The term "ribbon" describes the morphology of these organelles in photoreceptors and retinal bipolar neurons. In mechanosensory hair cells of the auditory and vestibular systems, the homologous organelles are known as synaptic bodies (SBs) and can have a variety of shapes from flat to spherical. To better understand the synaptic vesicle cycle and the role of the SB, we used three-dimensional reconstructions of afferent synapses in hair cells from the frog sacculus to study the steady-state redistribution of vesicles and other membrane-bounded compartments that takes place during long-lasting excitation or inhibition. These results can be compared to our previous study (Lenzi et al., 1999) in which we investigated the ultrastructure of the hair cell's afferent synapse in the resting state.

Electron tomography permits high-resolution 3D mapping of synaptic ultrastructure (Harlow et al., 1998, 2001), including the afferent synapses in frog saccular hair cells (Lenzi et al., 1999), with an order of magnitude better *z* axis resolution than is possible using serial thin sections. The improved resolution made it possible to unambiguously identify and trace the outlines of all membrane-bounded structures in a region of cytoplasm that is densely packed with synaptic vesicles and other organelles, many of which are smaller than the thickness of a thin section. It also allowed us to use a strict criterion to identify "morphologically docked vesicles," which could not have been applied in thin sections because the plasmalemma is not flat and thus was often oblique to the plane of section.

Docked synaptic vesicles are believed to include those that are first in line to fuse with the plasmalemma following the onset of a depolarizing stimulus at both conventional (Schikorski and Stevens, 1997; Li and Schwarz, 1999) and ribbon synapses (Mennerick and Matthews, 1996; von Gersdorff et al., 1998). They bind to the plasmalemma at the active zone by specific protein interactions (Brunger, 2000), and their number correlates with the size of the fastest phase of exocytosis (Stevens and Tsujimoto, 1995; Schikorski and Stevens, 1997).

Ultrastructural and physiological evidence suggests that docked vesicles at the active zone are replenished from the pool of vesicles tethered to the ribbon, possibly by the movement of vesicles along the SB surface (Harlow et al., 2001; see Lenzi and von Gersdorff, 2001). Labeled vesicles turn over on the ribbon (Schaeffer and Raviola, 1978; Siegel and Brownell, 1986), and capacitance measurements (von Gersdorff et al., 1998; Moser and Beutner, 2000) show that depolarization evokes an initial exocytic burst that may correspond to the fusion of previously docked vesicles with the plasmalemma, followed by a more sustained capacitance rise. In bipolar cells, the second phase ends after the fusion of the equivalent of the ribbon's complement of vesicles (von Gersdorff and Matthews, 1994; von Gersdorff et al., 1996), suggesting that release sites are replenished from the ribbon, but in hair cells, the capacitance rise continues long enough that the SB would have to be reloaded several times within a few seconds (Parsons et al., 1994; Lenzi et al., 1999; Moser and Beutner, 2000). The rate-limiting step during sustained exocytosis, and the exact role of the ribbon in the vesicle cycle, thus remain elusive. The ribbon could recruit vesicles from the cytoplasm (Morgans 2000), actively transport them to the active zone (Muresan et al., 1999), or have another role (Vollrath and Spiwoks-Becker, 1996).

Results

We subjected hair cells to 30 min of continuous stimulation or inhibition to either enhance or inhibit tonic transmitter release. We exposed the sensory epithelium of the frog sacculus to high-K^+ saline (30 or 45 mM K^+) (Zucca et al., 1992; Parsons et al., 1994) or 0-Ca^{2+} saline (2 mM EGTA with no added Ca^{2+}) before fixing and

[3]Correspondence: roberts@uoneuro.uoregon.edu
[4]Present address: Cytokinetics, Inc., South San Francisco, California, 94080.

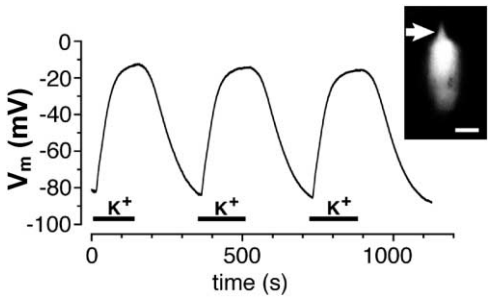

Figure 1. High-K^+ Saline Depolarizes Hair Cells In Situ

Intracellular microelectrode recording of hair cell membrane potential during perfusion of 45 mM K^+ saline (bars); normal saline containing 2 mM K^+ was perfused at other times. The last three of four K^+ applications are shown. The sensory epithelium had been dissected and furrowed as in preparations used for electron microscopy. The inset shows the fluorescence image of the same hair cell after filling with Lucifer yellow and withdrawal of the microelectrode. The apical hair bundle (arrow) identified this cell as a hair cell. Scale bar, 10 μm.

preparing the tissue for electron microscopy. Figure 1 shows that solution exchanges were effective within ~1 min and depolarized the cell by ~70mV, close to the expected change of 78mV calculated from the Nernst equation: $\Delta V = 58mV\ log(45/2)$. A 70mV depolarization is sufficient to massively activate the presynaptic calcium current (Roberts et al., 1990) and exocytosis (Parsons et al., 1994). Because the epithelium contains both hair cells and support cells, in a few cases we included a fluorescent dye in the recording pipette to identify the cell type (Figure 1, inset). Each of 12 cells, including 2 that we identified as hair cells and 2 as support cells, rapidly depolarized in high K^+. We conclude that small ions in the bathing medium have rapid and complete access to the synapses on the hair cells' basolateral surfaces in our experimental preparation.

We reconstructed seven synapses from four sacculi exposed to high-K^+ saline, and four synapses from three sacculi exposed to 0-Ca^{2+} saline (Table 1). Acquisition and analysis were performed blind for 7 of the 11 reconstructed synapses. Figure 2 shows the effects of stimulation and inhibition on presynaptic ultrastructure. The computed *x-y* planes (Figures 2A and 2B) resemble conventional transmission electron micrographs of these synapses (compare to Figures 4A and 4B), although the computed sections are much thinner (2.9 nm in Figure 2A, 2.7 nm in Figure 2B). Visible in these sections were numerous small clear-core vesicles that we designate as "synaptic vesicles," larger coated vesicles, mitochondria, and other membranous tubules and vacuoles that we designate collectively as cisterns. Comparison of Figures 2A and 2B shows a steady-state depletion of synaptic vesicles in cells depolarized by high K^+, but this and other differences are more easily seen by rendering the entire volumes (Figures 2C and 2D). In these views, the presynaptic cytoplasm lies above the plasma membrane (red) and contains the traced organelles. We identified every small, clear-core vesicle in each reconstructed volume and measured the diameter and coordinates of a sphere fit through the vesicle's largest cross-section, whether the vesicle membrane came within 30 nm of the SB in any section (SB-associated vesicles), and whether the vesicle membrane was in contact with the plasmalemma in at least one *x-y* section (docked vesicles). SB-associated vesicles are rendered in yellow (Figures 2–4); most are tethered to the SB (Lenzi et al., 1999). All other small, clear-core vesicles were classified as "outlying vesicles" and are rendered in green.

The SB had no apparent internal structure and was rendered as a hollow semitransparent object to better reveal its shape and the objects behind it. The two SBs in Figure 2 appear as truncated hollow spheres, open at the face of the physical tissue section. Only a portion of each SB (36%–78%, n = 11; Table 1) was captured in any one reconstruction. Coated vesicles (gold) were

Table 1. Synaptic Body Size, Vesicle Numbers, Volumes, and Membrane Abundance at Reconstructed Synapses

	Synaptic Body		Number of Vesicles Counted				Reconstructed Volume		Relative Vesicle Membrane Area			
			Docked		Not Docked							
Synapse #	Diameter (nm)	% Complete	SB	Outlying	SB	Outlying	Cytoplasm (μm³)	Cisterns (% Volume)	SB (%)	Outlying (%)	Coated (%)	Cisterns (%)
Inhibited												
1	363	54%	25	66	153	643	0.168	3.2	16.4	65.2	5.8	12.6
2	387	41%	25	13	130	168	0.108	3.7	32.4	37.8	8.7	21.1
3	390	58%	24	6	262	371	0.249	2.0	34.6	45.6	7.6	12.3
4	464	50%	42	23	160	247	0.211	0.2	38.5	54.2	5.8	1.5
	401 ± 22						0.736	2.3 ± 0.8	30.5 ± 4.9	50.7 ± 5.9	7.0 ± 0.7	11.9 ± 4.0
Stimulated												
5	430	45%	5	1	97	132	0.148	7.7	26.4	20.5	5.9	47.3
6	361	45%	6	–	63	–	–	–	–	–	–	–
7	361	46%	15	8	90	38	0.066	8.8	25.5	11.4	2.2	61.0
8	360	78%	11	2	128	69	0.175	10.0	21.6	11.0	7.9	59.5
9	363	67%	16	8	72	165	0.273	10.8	14.4	28.3	2.6	54.7
10	452	36%	5	7	124	87	0.118	21.5	24.1	17.6	8.4	49.8
11	410	62%	5	7	143	189	0.261	5.2	20.3	26.9	17.4	35.5
	391 ± 15						1.041	10.7 ± 2.3*	22.0 ± 1.8	19.3 ± 3.0**	7.4 ± 2.3	51.3 ± 3.8**

Means are shown ± SEM. Cytoplasm volumes were summed. Synapses 5 and 6 were contained in the same reconstruction. Statistical significance (H_0: inhibited mean = stimulated mean; 2–tailed t test), *$p < 0.05$; **$p < 0.001$.

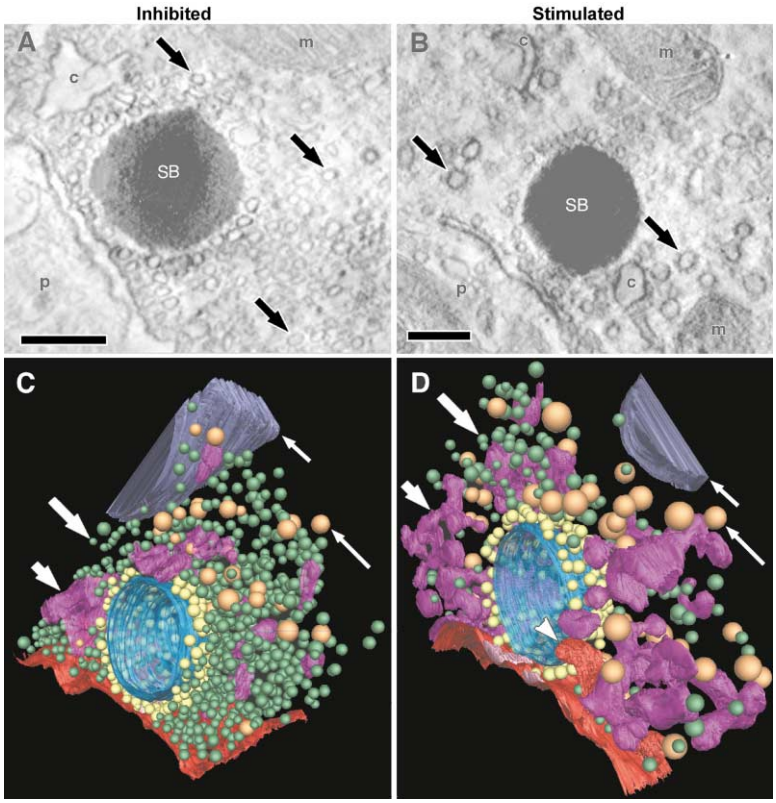

Figure 2. Stimulation Alters Hair Cell Afferent Synapse Ultrastructure

(A–D) Electron tomographic reconstructions of hair cell synapses exposed to 0-Ca^{2+} saline (A and C) or high-K^{+} (B and D) saline. (A and B) Single *x-y* planes through the reconstructed volumes are shown. The hair cell cytoplasm contains the synaptic body (SB) surrounded by synaptic vesicles, outlying cytoplasmic vesicles (arrows in [A]), coated vesicles (arrows in [B]), membrane-bounded cisterns (c), and mitochondria (m). The synaptic cleft is visible between the SB and the postsynaptic cell (p). (C and D) Three-dimensional structure of presynaptic organelles from the same reconstructions shown in (A) and (B). The SB (blue) was rendered as hollow and semitransparent and lies adjacent to the hair cell's plasma membrane (red). SB-associated vesicles (yellow) surround the SB; outlying vesicles (green, thick long arrows) lie further out in the cytoplasm. Also visible are coated vesicles (gold, thin long arrows), cisterns (purple, thick short arrows), and mitochondria (blue, thin short arrows). In (D), regions of presynaptic density (pink) lie beneath the SB on the plasma membrane, which formed a tubular invagination (arrowhead). The flat surfaces of the mitochondria and the open face of the SBs denote the edges of the reconstruction. In black and white copies of color figures, yellow appears lighter than green. Synapses 1 and 11; scale bars, 200 nm.

identified by the presence of an electron-dense coat (Figure 2B, arrows). For computational economy, both coated vesicles and synaptic vesicles were rendered as ideal spheres. Also visible are networks of interconnected cisterns (magenta), which were especially abundant and complex following stimulation (see below).

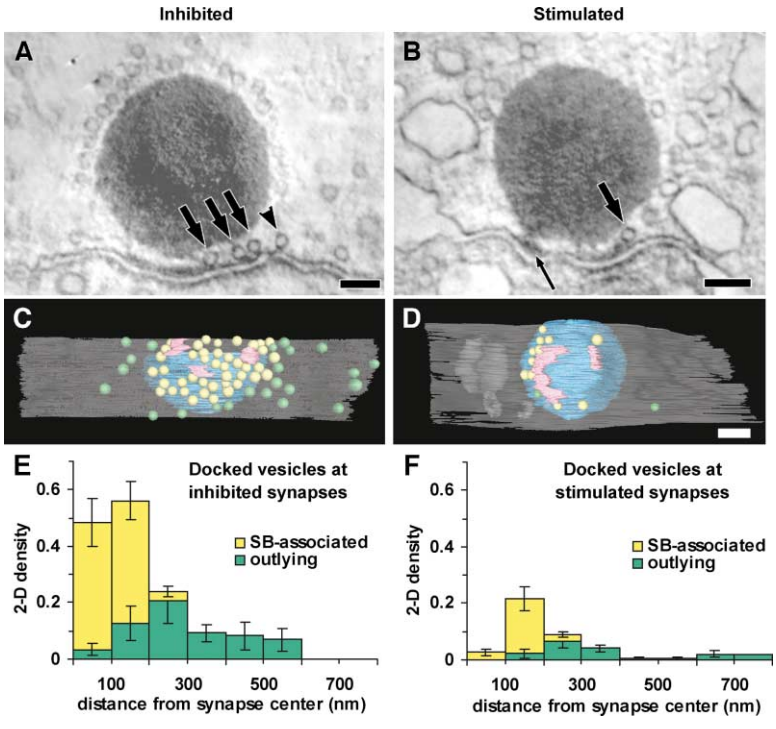

Figure 3. Depolarization Depletes Docked Vesicles

Reconstructions of synapses exposed to 0-Ca^{2+} saline (A and C) or high-K^{+} saline (B and D). Representative *x-y* planes (A and B) show morphologically docked vesicles at the plasma membrane beneath (arrows) or near (arrowhead) the electron-dense SB, and regions of presynaptic density (thin arrow). The docked vesicle in (B) illustrates that vesicles did not always touch the membrane in the plane in which they appeared largest. This vesicle is cut at its equator, but touched the plasmalemma in another *x-y* plane, 8 nm away. (C and D) Renderings of the same synapses, showing only the SB (blue), docked SB-associated vesicles (yellow), docked outlying vesicles (green), and regions of presynaptic density (pink) through a transparent plasma membrane (gray). Synapses 4 and 8; scale bars, 100 nm. Scale bar in (D) also applies to (C). (E and F) Stacked bar graphs showing the average density distributions of SB-associated docked vesicles (yellow) and outlying docked vesicles (green) from four synapses in 0 Ca^{2+} (E) and seven synapses in high K^{+} (F). Vesicle densities are expressed as a fraction of close-packed (see Experimental Procedures), and are plotted against the distance from the projected center of the SB. Error bars show SEM.

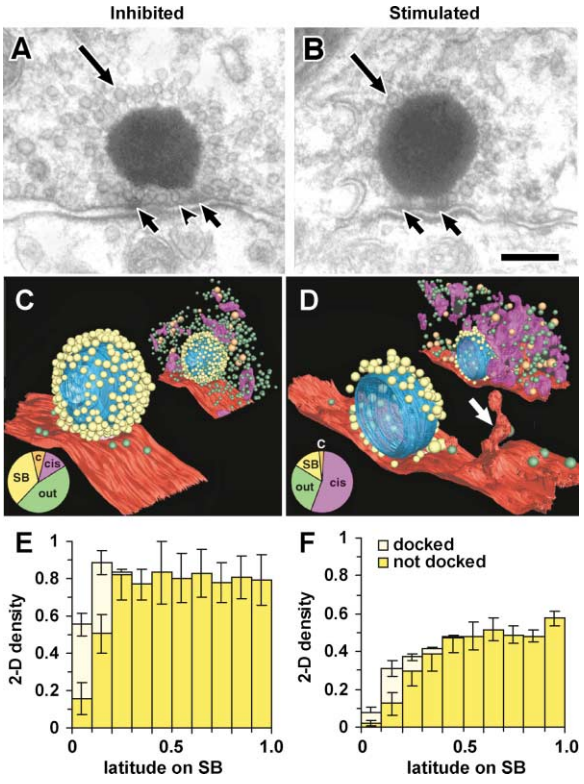

Figure 4. Depolarization Partially Depletes SB-Associated Vesicles and Redistributes Membrane

(A and B) Conventional transmission electron micrographs of synapses incubated in 0-Ca^{2+} saline (A) or high-K^+ saline (B). Vesicles surround the SB (long arrows) and are seen in the space between the SB and plasma membrane at inhibited synapses (arrowhead in [A]). This space also contains regions of presynaptic density (short arrows). Scale bar, 200 nm.

(C and D) Electron tomographic reconstructions of synapses exposed to 0 Ca^2 (C) and high K^+ (D). Renderings show the plasma membrane (red) in relation to the SB (blue), SB-associated vesicles (yellow), and docked outlying vesicles (green). In (D), the plasma membrane forms a tubular invagination (arrow). Upper insets show all traced organelles at these two synapses. Pie charts show the relative distribution of membrane area between compartments (SB, SB-associated vesicles; out, outlying vesicles; c, coated vesicles; *cis*, cisterns). The renderings correspond to synapse 3 (C) and synapse 9 (D) in Table 1.

(E and F) Stacked bar graphs showing average 2D packing density of SB-associated vesicles as a function of latitude on the SB are shown. Depolarization in high K^+ created a vesicle gradient on the SB surface. Error bars show SEM.

Depolarization Depletes Docked Vesicles

We observed numerous docked vesicles in the space between the SB and the plasmalemma at inhibited synapses (arrows, Figures 3A and 3B). We also counted many outlying docked vesicles, some of which were located hundreds of nanometers from the SB. Steady-state depletion of both SB-associated and outlying docked vesicles is readily apparent by comparing face-on views of stimulated and inhibited synapses (Figures 3C and 3D). In the two reconstructions shown, there were five times more docked vesicles at the inhibited synapse (Figure 3C) than at the stimulated synapse (Figure 3D), even though the stimulated synapse was more complete.

To make quantitative comparisons across synapses that varied in the completeness of the SB, area of plasmalemma, and volume of cytoplasm reconstructed, we computed the density of synaptic vesicles as a function of their position relative to the SB and plasmalemma. For docked vesicles, position was measured as the distance from the center of the active zone, defined by the line drawn perpendicular to the membrane plane through the center of a sphere fit to the SB. Vesicle density was expressed as a fraction of the maximum 2D packing density of 40 nm diameter spheres on a plane (Figures 3E and 3F). To take into account the fact that some vesicles are expected to lie close to the plasmalemma even without any specific binding interaction, we estimated the frequency of random close encounters based on the density of vesicles in the cytoplasm and the spatial resolution of our computed tomographic sections (see Experimental Procedures). The estimated frequency of random close encounters was small: $<0.5\%$ of dense-packed in high K^+ (where cytoplasmic vesicles were sparse) and $<2\%$ of dense-packed in 0-Ca^{2+} (where cytoplasmic vesicles were abundant). We conclude that almost all of the docked vesicles that we counted were specifically associated with the plasma membrane.

At inhibited synapses, docked vesicles covered $\sim$50% of the membrane area within a radius of 200 nm of the active zone center (Figure 3E). Most of these central docked vesicles were SB associated (yellow bars). Outlying docked vesicles (green bars) generally occurred at much lower density and were most abundant in an annulus around the periphery of the active zone (between 200 and 300 nm from the center).

To estimate the total number of docked vesicles within 800 nm of the active zone center, we integrated the vesicle density distributions, assuming radial symmetry. Surprisingly, at inhibited synapses we estimate that outlying docked vesicles, which were scattered at low density over a large area, were twice as numerous as SB-associated docked vesicles, which were tightly packed into a small area (Table 2). Stimulation depleted both SB-associated and outlying docked vesicles in approximately equal proportions (Table 2).

Depolarization Partially Depletes SB Vesicles and Creates a Gradient of Vesicles on the SB

We used both conventional transmission electron microscopy (TEM; Figures 4A and 4B) and electron tomography (Figures 4C–4F) to study SB-associated vesicles. In a survey of TEM sections from 48 stimulated synapses and 48 inhibited synapses, we found a modest (21%) but statistically significant ($p < 0.001$) decrease in the 1D density of vesicles along the perimeter of the SB (Figure 4B), similar to the noise-induced depletion reported in lizard hair cells (Henry and Mulroy, 1995). Vesicles were plentiful around the entire perimeter of all SBs, except that following stimulation, they were rarely seen in the space between the SB and the plasmalemma. For some of these TEM experiments, the 0-Ca^{2+} or high-K^+ saline was chilled on ice during the incubation in an attempt to block vesicle recycling (Schaeffer and Raviola, 1978). In these cells, the 1D packing densities of SB-associated vesicles were 0.63 $\pm$ 0.03 in 0 Ca^{2+}

Table 2. Estimated Total Number of Vesicles in Each Class within 800 nm Radius of a Complete Active Zone

	SB, Docked	Outlying, Docked	SB, Not Docked	Outlying, Not Docked	Total Docked	Total Not docked	Total SB	Total Outlying	Total
Inhibited	43 ± 8	81 ± 37	357 ± 42	1997 ± 320	124 ± 34	2354 ± 314	400 ± 44	2078 ± 344	2478 ± 329
Stimulated	16 ± 2	21 ± 6	198 ± 29	427 ± 82	39 ± 8	632 ± 79	215 ± 29	448 ± 84	671 ± 80
% Depletion	62 ± 9%***	74 ± 30%^{NS}	44 ± 11%**	79 ± 6%***	68 ± 13%*	73 ± 5%***	46 ± 10%***	78 ±6%***	73 ± 5%***

Values (mean ± SEM) were obtained by integrating the vesicle density functions shown in Figures 4G and 4H (SB-associated vesicles), Figures 3E and 3F (outlying docked vesicles), and Figures 5A and 5B (outlying nondocked vesicles); n = 4 for inhibited synapses; n = 7 for SB-associated vesicles at stimulated synapses; n = 5 for outlying vesicles at stimulated synapses. Synapses 5 and 6 were not used for outlying vesicle calculations because they were located within 800 nm of each other. Statistical significance (H_0: inhibited mean > stimulated mean; 1-tailed t test), ***$p < 0.005$; **$p < 0.01$; *$p < 0.025$; NS, $p > 0.05$

(mean ± SEM; 305 vesicles at 19 synapses from 2 sacculi) and 0.55 ± 0.02 in high K^+ (571 vesicles at 39 synapses from 6 sacculi). The corresponding densities in cells incubated at room temperature were not significantly different ($p > 0.1$): 0.67 ± 0.03 in 0 Ca^{2+} (605 vesicles at 29 synapses from 5 sacculi) and 0.48 ± 0.03 in high-K^+ (143 vesicles at 9 synapses from 2 sacculi). At both temperatures, depolarization caused a significant depletion of SB-associated vesicles ($p < 0.001$).

In tomographic reconstructions we saw a higher density of SB-associated vesicles at inhibited synapses and more depletion at stimulated synapses than we saw in TEM sections (3D packing density: 0.79 ± 0.09, inhibited; 0.42 ± 0.04, stimulated). These densities are converted to vesicle counts in Table 2. We believe that the tomographic data are more accurate than the TEM counts and attribute the differences largely to the failure to count all superimposed vesicles in TEM sections. Superimposed vesicles are expected to occur frequently, given their high density on the SB and because the section thickness exceeded the vesicle diameter.

To analyze the distribution of vesicles on the surface of the SB, we fit a sphere to the SB and defined latitude relative to the same axis used to define the center of the active zone. The pole closest to the plasmalemma was defined as the membrane pole, the other the cytoplasmic pole. The SB surface was then divided into ten latitude bands of equal surface area, corresponding to ten equally spaced bins of the axial coordinate (z), normalized such that $z = 0$ at the membrane pole, $z = 0.5$ at the equator, and $z = 1$ at the cytoplasmic pole. The 2D density of SB vesicles as a function of z is shown in Figures 4E and 4F. We integrated these density distributions to estimate the number of SB-associated vesicles per complete SB. Depolarization significantly depleted both docked and nondocked vesicles on the SB (Table 2) without altering the SB diameter (Table 1).

Counting both docked and nondocked vesicles together, vesicles at inhibited synapses were distributed nearly uniformly on the SB (Figure 4E) except for a small (~20%) reduction in vesicle density near the membrane pole ($z < 0.1$), which is consistent with vesicles being excluded from space occupied by the presynaptic densities (Figures 3C and 3D). After stimulation (Figure 4F), the distribution was markedly nonuniform, with an 86% depletion of vesicles in the bin surrounding the membrane pole ($z < 0.1$), but only 37% average depletion across the opposite hemisphere ($z > 0.5$). Comparison of Figures 4E and 4F shows that both docked and nondocked vesicles were depleted. For statistical analysis, we normalized vesicle densities on each SB to the mean for that SB (i.e., a normalized density of 1 corresponds to the mean density of vesicles on the SB; both docked and nondocked vesicles were included). In inhibited cells, an analysis of variance (ANOVA) showed no significant effect of latitude ($p > 0.5$; n = 4 synapses) and no significant correlation between z and normalized vesicle density ($R = 0.09$; $p > 0.5$). In stimulated cells, there was a highly significant effect of latitude (ANOVA, $p < 10^{-5}$; n = 7 synapses) and a significant correlation ($R = 0.63$; $p < 10^{-8}$); this significance persisted if the bin at the membrane pole ($z < 0.1$) was eliminated from the analysis (ANOVA, $p < 0.025$; correlation, $R = 0.48$; $p < 10^{-4}$). We then proceeded to make t tests (single sample, two-tailed) to assess whether the vesicle density in each of the ten latitude bins was significantly above or below average. The greatest deviations were observed at the membrane pole ($z < 0.1$), where the normalized vesicle density was significantly less than 1 ($p < 0.0005$), and the cytoplasmic pole ($z > 0.9$), where the density was significantly greater than 1 ($p < 0.01$). Vesicle densities were also significantly elevated in the two bins between $z = 0.7$ and $z = 0.9$ ($p < 0.05$).

Because it has been hypothesized that movement of nondocked vesicles on the SB surface occurs during the vesicle cycle, we were particularly interested in any changes in their distribution caused by stimulation. Analysis of nondocked SB vesicles was confounded by the gradient seen in inhibited cells (Figure 4E), which remained even after we subtracted the space occupied by docked vesicles from the reconstructed SB area in each bin (ANOVA, $p < 0.005$; correlation, $R = 0.36$, $p < 0.025$). However, this gradient at inhibited synapses was due entirely to a deficiency of nondocked vesicles close to the membrane pole ($z < 0.1$) and may simply reflect the space occupied by the presynaptic densities. After eliminating the bin at the membrane pole from the analysis, there was no significant effect of latitude on the density of nondocked SB vesicles (ANOVA, $p > 0.9$; correlation, $R = 0.09$, $p > 0.6$; vesicle densities corrected for space occupied by docked SB vesicles). In contrast, there was a highly significant gradient of nondocked SB vesicles in stimulated cells, regardless of whether the bin at the membrane pole was included in the analysis (ANOVA, $p < 0.0005$; correlation, $R = 0.48$, $p < 10^{-4}$; bin at membrane pole excluded, corrected for space occupied by docked SB vesicles).

It is possible that vesicles associate and dissociate from the SB more rapidly than they can move along its surface; in which case, the gradient of SB vesicles in

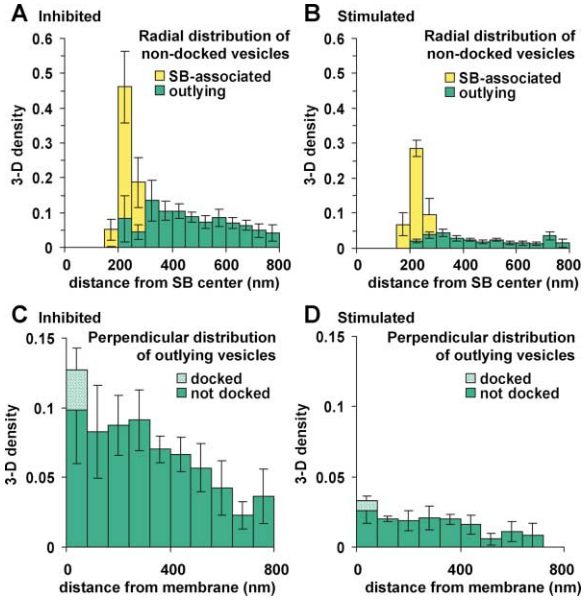

Figure 5. Stimulation Depletes Vesicles within 800 nm of the Active Zone

(A and B) Density of nondocked vesicles as a function of radial distance from the SB center at inhibited (A) and stimulated (B) synapses. Outlying vesicle density decreased with distance from the SB at both inhibited and stimulated synapses.

(C and D) Density of outlying vesicles as a function of perpendicular distance from the plasmalemma at inhibited (C) and stimulated (D) synapses, excluding a 300 nm radius cylinder centered on the SB. The density of nondocked vesicles was constant within ~300 nm of the membrane and declined farther away; depletion was evident up to the largest distance included in this study. Stacked bar graphs; error bars show SEM

stimulated cells could reflect a gradient of nearby outlying vesicles. To test this possibility, we calculated the 3D density of outlying vesicles as a function of z in a 40 nm thick shell surrounding the SB-associated vesicles. We were unable to make meaningful measurements for $z < 0.2$ because most of this volume fell outside of the hair cell, but outlying vesicle densities at higher latitudes showed either no clear spatial gradient or one opposite to that seen for SB-associated vesicles. At inhibited synapses, the density of outlying vesicles was 0.17 close to the membrane ($0.2 < z < 0.3$) and declined smoothly to a value of 0.035 at the opposite pole. At stimulated synapses, the density was between 0.025 and 0.095, with no significant relationship to latitude. There was no significant correlation between the density of nondocked SB-associated vesicles and the density of nearby outlying vesicles (inhibited, $R = -0.2$; $p > 0.6$; stimulated, $R = -0.5$; $p > 0.2$).

Depolarization Depletes Outlying Vesicles and Redistributes Membrane

The renderings in Figures 2 and 4 show fewer outlying vesicles at stimulated synapses than at inhibited synapses (Table 1). To quantify the spatial extent of vesicle depletion, we estimated the 3D density of vesicles in the cytoplasm as a function of radial distance from the SB center (Figures 5A and 5B), and integrated this distribution to estimate the total number of vesicles within a radius of 800 nm (Table 2). We also calculated vesicle density as a function of perpendicular distance from the plasmalemma (Figures 5C and 5D). Depolarization depleted vesicles at all distances from the synapse center or plasmalemma, up to the largest distances that we could study in the rendered volumes.

To determine the fate of membrane lost from the synaptic vesicle compartments during depolarization, we estimated the surface area of all membrane-bounded organelles in the reconstructions. The SB surface area was not included because a membrane does not delimit it. The pie charts in Figure 4 give the relative membrane areas of vesicle and cistern compartments for two synapses. In 0 Ca^{2+} (Figure 4C), small uncoated vesicles (SB and out) accounted for four-fifths of the membrane, while the remaining one-fifth was contained in cisterns and coated vesicles. The distribution of membrane was dramatically different in the synapse exposed to high K^+. Here (Figure 4D) cisterns were more numerous, had more complex shapes, and accounted for more than half the total membrane area, while the contribution from vesicles, particularly outlying synaptic vesicles, fell. Table 1 shows the averaged data for all synapses. Depolarization increased the average fraction of cistern membrane by more than 4-fold, while the contributions of outlying and SB vesicle membrane fell by approximately one-half and one-third, respectively. Relative changes in outlying vesicle and cistern surface areas were statistically significant ($p < 0.001$). The fraction of coated vesicle membrane was unchanged by depolarization.

To determine whether depolarization redistributed a fixed amount of membrane, we next considered an absolute measure of membrane abundance, normalized to the available volume. We calculated the concentration of membranes in the reconstructed volumes by dividing organelle surface area by the volume of hair cell cytoplasm not occupied by the SB or mitochondria. Figure 6A compares average membrane concentrations at stimulated and inhibited synapses. Depolarization-induced changes in membrane concentration paralleled the changes in relative membrane abundance. Changes in the concentrations of outlying vesicle membrane and cisternal membrane were largest and were statistically significant ($p < 0.005$). The concentration of SB-associated vesicle membrane changed less, but was still significant ($p < 0.05$). The coated vesicle compartment remained unchanged ($p > 0.5$).

Previously, we (Lenzi et al., 1999) and others (Hama and Saito 1977) observed plasma membrane infoldings near hair cell synapses. Here, we found the plasma membrane to be smooth at inhibited synapses and considerably more convoluted following 30 min of depolarization (compare Figures 4C and 4D). Plasmalemmal infoldings (Figures 6B–6F) were highly correlated with depolarization, 16 occurring among 7 depolarized synapses, but with only 1 among 4 inhibited synapses. We quantified the surface area of these infoldings, including pits (Figure 6D), tubules (Figure 6F), and more complex structures (Figures 6B, 6C, and 6E). While these infoldings contributed only a small fraction of total membrane area (Figure 6A), they were significantly more abundant at high-K^+-exposed synapses ($p < 0.02$; Figure 6A, inset). As reported previously in goldfish saccular hair cells (Hama and Saito, 1977), we also found evi-

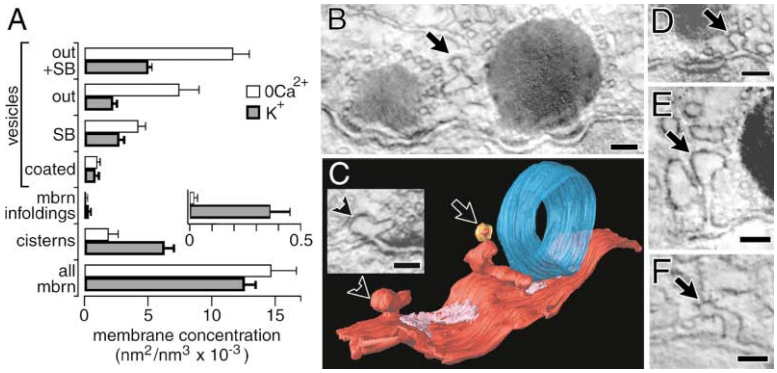

Figure 6. Depolarization Redistributes Membrane between Compartments and Invaginates the Plasma Membrane

(A) Average membrane concentrations of presynaptic organelles after 0-Ca^{2+} or high-K^+ treatment. Concentrations are shown for coated, SB-associated, outlying, and the sum of outlying and SB-associated vesicles. The abundance of plasma membrane infoldings (also shown on an expanded scale in the inset), cistern membrane, and the sum of all compartments are also shown. Bars denote averages computed from all the tomographic reconstructions; error bars show SEM.

(B–F) Portions of reconstructed synapses exposed to high K^+ showing plasma membrane invaginations. Electron dense SBs are visible in (B–E). (B) A coated bud (arrow) forming from a convoluted plasma membrane invagination between two synapses. (C) Rendering of the same reconstruction as (B), showing the coated bud (gold, arrow) connected to the plasmalemma (red). Only one SB (blue) is shown for clarity; regions of presynaptic density (pink) are shown for both synapses. The arrowheads show a club-shaped membrane invagination, in the rendering and in an x-y plane (inset). (D) Coated pit (arrow) adjacent to the SB. (E) Deep, tubular plasma membrane invagination adjacent to the SB (rendered in Figure 1D). (F) Coated pit forming from a short plasma membrane invagination. Synapses 5 and 6 (B and C), 7 (D), and 11 (E and F). Scale bars, 50 nm in (F), 100 nm elsewhere.

dence for coated pits budding from these invaginations (Figures 6B, 6C, and 6F), suggesting that these provide a route for membrane retrieval by endocytosis through a coated vesicle pathway.

We next asked whether vesicle membrane depleted by stimulation could be accounted for by increases in the surface areas of other organelles. Total membrane lost from synaptic vesicle compartments during depolarization is shown by the difference between the topmost bars in Figure 6A. Approximately 75% of this difference can be accounted for by the increase in cisterns, and to a much lesser extent, plasmalemma infoldings, the only two compartments that increased in stimulated cells. Total membrane concentrations (bottom bars, Figure 6A) were not significantly different between stimulated and inhibited cells ($p > 0.29$), consistent with the local conservation of membrane that is redistributed among compartments upon depolarization.

Coated vesicles were unaffected by depolarization, and their relative (Table 1) or absolute (Figure 6A) total average surface areas were not altered. Their number per synapse (18 ± 4 in 0 Ca^{2+}; 22 ± 6 in high K^+) and average diameters (52.5 ± 1.4 nm, $n = 79$ in 0 Ca^{2+}; 53.5 ± 0.9 nm, $n = 131$ in high K^+) were also unaffected by depolarization.

Discussion

Some sensory systems reduce the loss of information that occurs when continuous, graded inputs are converted into all-or-none action potentials by performing the initial signal processing in receptor cells and interneurons that do not generate spikes (for review, see Juusola et al., 1996). To transmit information contained in graded membrane potential changes, the output synapses must be sensitive to depolarizations that are much smaller than an all-or-none action potential. In some cases, the synapses are also "tonic" (i.e., they do not adapt completely during a maintained depolarization) and can thus transmit steady-state sensory information (Lagnado et al., 1996; Glowatzki and Fuchs, 2002). Ribbon-class synapses perform these functions in the eyes, ears, and lateral line organs of vertebrate animals.

Ribbon synapses resemble typical fast chemical synapses in some respects, but differ in others. In hair cells, exocytosis of transmitter stored in small clear-core synaptic vesicles is controlled by intracellular Ca^{2+} (Moser and Beutner, 2000; Beutner et al., 2001) that enters through voltage-gated Ca^{2+} channels, creating quantal postsynaptic responses (Furukawa et al., 1982; Glowatzki and Fuchs, 2002). However, the threshold Ca^{2+} concentration is somewhat higher than at other synapses (Mennerick and Matthews, 1996; Beutner et al., 2001), the Ca^{2+} channels are of an unusual type, and the frequent occurrence of large quantal responses suggests multivesicular release (Glowatzki and Fuchs, 2002). The core fusion complex contains some components in common with other synapses but lacks synaptotagmin I and II; synapsins are also absent (Lenzi and von Gersdorff, 2001). Other proteins may be unique to ribbon synapses (Schmitz et al., 2000). As expected for tonic transmission, exocytosis is controlled by Ca^{2+} influx through noninactivating Ca^{2+} channels (Spassova et al., 2001; see Juusola et al., 1996). Hair cells express splice variants of the L-type Ca^{2+} channel α_{1D} subunit (Cav1.3) (Kollmar et al., 1997a, 1997b; Hibino et al., 2002) that activate very rapidly and at more negative membrane potentials than other L-type channels, allowing them to control transmitter release in response to small, fast sensory signals. They also show little or no inactivation, although this property may require additional subunits or posttranslational modification (Koschak et al., 2001).

We incubated hair cells for 30 min in high-K^+ or 0-Ca^{2+} saline, to allow time to reach a steady state before fixation. We did not measure postsynaptic responses or membrane cycling, and therefore do not know the extent to which transmitter release may have declined during such a long depolarization, but similar stimulation elicited exocytosis that lasted the duration of the experiment in cochlear hair cells ($\sim$3 min) (Glowatzki and Fuchs, 2002) and retinal bipolar cells ($\sim$10 min) (Lagnado et al., 1996; for a conflicting view, see Rouze and Schwartz, 1998). For every metric compared, including the densities of docked, SB-associated, and outlying vesicles, as well as the abundance of putative endocytic sites, our measurements from cells incubated in high

K^+ or 0 Ca^2 bracketed those from cells incubated in normal extracellular saline containing 2 mM K^+ and 4 mM Ca^{2+} (Lenzi et al., 1999). We conclude that high K^+ enhanced, and 0 Ca^{2+} inhibited synaptic transmission relative to the ongoing release that occurs at rest. Overall, stimulation caused a shift of membrane from small, clear-core vesicles into other compartments. Membrane accumulated primarily in irregularly shaped cisterns, suggesting that the formation of new synaptic vesicles from cisternal membrane was the rate-limiting step during continuous membrane recycling. A possible alternative explanation is that exocytosis stopped at some point during the incubation in high K^+, but the ultrastructure did not return to the resting state, perhaps because high-intracellular Ca^{2+} blocks the formation of new vesicles.

Functional models of ribbon synapses have attempted to link their prominent anatomical feature—the synaptic ribbon or synaptic body—with their ability to sustain a high rate of continuous exocytosis (for review, see Lenzi and von Gersdorff, 2001). Many investigators have hypothesized the ribbon to be a transport device that somehow helps to rapidly replenish release sites (Bunt, 1971; Gray and Pease, 1971). Capacitance measurements in retinal bipolar neurons (von Gersdorff et al., 1996; Mennerick and Matthews, 1996) have led to a refinement of this model, in which it is proposed that strong depolarization evokes the rapid exocytosis of all docked vesicles at the active zone, followed by a slower phase that continues until the remaining supply of ribbon-associated vesicles is exhausted. Exocytosis might then stop entirely or continue at an even slower pace (limited by the rate at which vesicles repopulate the SB) that is undetectable in capacitance experiments because this technique measures the difference between exocytosis and endocytosis, which is zero in the steady state. We found that 30 min in high K^+ caused a large depletion of docked vesicles as predicted, but only a modest depletion of SB-associated vesicles. This may reflect a real difference between hair cells and bipolar cells. Capacitance measurements from hair cells have not identified a kinetic component of exocytosis that could correspond to depletion of SB-associated vesicles (Parsons et al., 1994; Moser and Beutner, 2000).

When exocytosis is inhibited, vesicles populate the entire SB surface at near close-pack densities (Figure 4E). Maximal stimulation causes a massive (86%) depletion of both docked and nondocked vesicles near the membrane pole (Figures 4E and 4F; Figures 3E and 3F; $z < 0.1$ in Figure 4 corresponds to a radius of $\sim$145 nm in Figure 3). The partial (37%) depletion of SB vesicles from the cytoplasmic hemisphere indicates that these SB vesicles are also involved in the vesicle cycle (Schacher et al., 1974, 1976; Schaeffer and Raviola, 1978, Siegel and Brownell, 1986; Henry and Mulroy, 1995), and the lack of correlation between the density of vesicles on the SB and in the adjacent cytoplasm rules out the possibility that the gradient of SB-associated vesicles is created by an equilibrium with a gradient of surrounding outlying vesicles. This result is consistent with evidence that vesicles do not readily detach from the SB (Schmitz et al., 1996; Lenzi et al., 1999).

The presence of a large gradient of SB-associated vesicles in stimulated cells suggests that any movement of vesicles along the surface of the SB is too slow to keep pace with maximum rate at which they can fuse with the plasmalemma. In the simplest scenario, the relatively slow movement (either by diffusion or directed transport) of vesicles along the SB to release sites, followed by their rapid exocytosis, establishes a standing concentration gradient. Alternatively, the recent work of Glowatzki and Fuchs (2002) raises the possibility that SB-associated vesicles can fuse with the plasmalemma without first moving to the active zone. One explanation for the large postsynaptic currents that they interpret as "multivesicular" fusion events is that several SB-associated vesicles fuse with each other either before or simultaneously with one of them fusing with the plasmalemma. A single exocytic event could thus eliminate a chain of up to 20 vesicles, which would extend far up the SB. In this scenario, some of the tubules that we observed near the SB in stimulated cells could be the remnants of such multivesicular fusions.

Physiological measurements in goldfish saccular hair cells suggested two types of release sites (Furukawa et al., 1982). According to their model, vesicles docked directly beneath the membrane pole of the SB are the first to undergo exocytosis, but cannot be replenished rapidly because incoming vesicles preferentially dock at more accessible sites at the periphery of the SB. The results shown in Figures 3E and 3F support this hypothesis. In stimulated cells, the density of all docked vesicles in the annulus between 100 and 200 nm surrounding the SB center was 5.8 ± 2.2 (mean $\pm$ SEM) times the density of all docked vesicles within 100 nm of the SB, compared to a ratio of 1.2 ± 0.1 in inhibited cells. This difference between stimulated and inhibited cells was statistically significant (one-tailed t test; $p < 0.02$).

One surprising finding was that two-thirds of the docked vesicles within an 800 nm radius of the active zone center are not associated with the SB (Table 2). Unlike the SB-associated vesicles, which face glutamate receptors in the postsynaptic membrane (Matsubara et al., 1999) and lie adjacent to regions of presynaptic (Figures 3C and 3D) density that may correspond to the locations of presynaptic calcium channels (Roberts et al., 1990), outlying vesicles are poorly situated to participate in synaptic transmission. Nevertheless, all docked vesicles were greatly depleted at stimulated synapses. Although the rise in intracellular Ca^{2+} concentration associated with normal synaptic transmission may be restricted to the active zone (Roberts, 1994), it is possible that the long depolarizations used here caused a more widespread elevation of intracellular Ca^{2+} that was able to trigger exocytosis hundreds of nanometers away. In retinal bipolar cells, single vesicles can fuse outside of hot spots, consistent with occasional exocytosis away from the ribbon in these cells as well (Zenisek et al., 2000). A similar mechanism was proposed by Beutner et al. (2001) to account for the large pool vesicles available for release when flash photolysis of caged Ca^{2+} was used to rapidly elevate Ca^{2+} throughout the cytoplasm. Our data cannot resolve unambiguously whether either class of docked vesicles disappear because they fuse with the plasma membrane or instead undock and rejoin the cytoplasmic pool as reported at CNS synapses (Murthy and Stevens, 1999) and in retinal bipolar cells (Zenisek et al., 2000), but the appearance of numerous membrane infoldings and coated pits in stimulated cells indicates that many of the docked vesicles fuse with the plasmalemma.

Electron tomography also permitted mapping the distribution of outlying vesicles in the synaptic cytoplasm. Outlying vesicles accumulated in the cytoplasm near the SB (Figures 5A and 5B) (Lenzi et al., 1999) at both inhibited and stimulated synapses. This gradient is opposite to what is expected if vesicles reach the SB by free diffusion, and suggests that some process operates to concentrate outlying vesicles within a few hundred nanometers of the SB. This could involve active transport or the binding of vesicles to cytoplasmic sites that are themselves concentrated near the SB. Alternatively, the SB could be the site for formation of new vesicles, which then diffuse away.

Despite a pronounced stimulation-driven redistribution of membrane from synaptic vesicles into cisterns and plasmalemmal infoldings, the total membrane concentration in the vicinity of the active zone remained nearly constant (Figure 6A). The conservation of membrane area and the appearance of structures associated with membrane retrieval near the active zone suggests that much of the recycling of synaptic vesicle membrane occurs locally at each synaptic site, although membrane may be retrieved at distant sites as well (Griesinger et al., 2002). The presence of coated pits and coated vesicles near the active zone (Heuser and Reese, 1973; Gad et al., 1998) suggests that clathrin-mediated endocytosis is prevalent in hair cells from frogs (Jacobs and Hudspeth, 1990; Lenzi et al., 1999), mammals (Siegel and Brownell 1986; Nadol, 1990), and fish (Hama and Saito, 1977). In the present experiments, coated pits, as well as deeper, more complex infoldings (Hama and Saito 1977), were much more abundant in stimulated cells than in inhibited cells or resting cells (Lenzi et al., 1999). It is conceivable that these tubular invaginations could pinch off whole, thus importing large amounts of membrane at once. Despite the marked increase in the number of coated pits, there was no concomitant increase in coated vesicles in the cytoplasm, which suggests that uncoating and/or fusion with an endosome are not rate-limiting steps.

Synaptic vesicles have been proposed to derive either from membrane recycled through an endosome compartment or directly from clathrin-coated vesicles (reviewed by Brodin et al., 2000). In frog saccular hair cells, coated vesicles are unlikely to be the direct source of new synaptic vesicles because their diameter was on average 1.6× larger. Very few coated vesicles were in the size range of synaptic vesicles. Previous studies have shown activity-dependent increases in cytoplasmic membrane compartments at the neuromuscular junction (Heuser and Reese, 1973), central synapses (Leenders et al., 2002), and in hair cells (Mulroy et al., 1990), consistent with the accumulation of membrane in an endosome compartment (Richards et al., 2000). In the present experiments, the increase in irregularly shaped intracellular compartments that we have called "cisterns" accounted for most (~75%) of the membrane lost from vesicles, suggesting that, at least during prolonged maximal stimulation, cisterns are an important component of the recycling pathway; other pathways may also operate at ribbon synapses (Lagnado et al., 1996; von Gersdorff and Matthews, 1997; Rouze and Schwartz, 1998).

Ribbon synapses are specialized for sustained, continuous exocytosis in nonspiking neurons and sensory cells. During maximal sustained stimulation, resupply of vesicles to the plasmalemma is evidently unable to keep pace with the maximal rate of exocytosis, resulting in a dramatic depletion of docked vesicles, and creating a vesicle gradient on the SB. However, the accumulation of membrane in cisternal compartments indicates that it is the reformation of new vesicles from cisternal membrane, rather than the reloading of docking sites, formation of SNARE complexes (Zenisek et al., 2000), or ATP-dependent priming of docked vesicles (Heidelberger, 1998) that is the overall rate-limiting step in this cycle.

Experimental Procedures

Statistics

Standard statistical methods were employed to test for significant differences between experimental conditions (see text). Averages are expressed as the mean ± SEM.

Electron Microscopy

We studied hair cells from the sacculus of the frog, *Rana pipiens*. Sacculi were removed from the inner ear and the sensory epithelium dissected free of the otolith in low-Ca^{2+} saline containing 110 mM Na^+, 2 mM K^+, 0.05 mM Ca^{2+}, 112.1 mM Cl^-, 5 mM HEPES, and 3 mM D-glucose. Ca^{2+} was omitted for the saline used in some dissections. The otolithic membrane was then removed, and the epithelium maintained at room temperature for 15–80 min in the dissection saline before furrowing the tissue to disrupt the apical diffusion barrier (Armstrong and Roberts, 1998; Lenzi et al., 1999). The furrowed epithelium was incubated for an additional 0–30 min in normal (2–4 mM Ca^{2+}) extracellular saline before switching to either high-K^+ or 0-Ca^{2+} saline for 30 min. High-K^+ saline contained 45 mM K^+ and was derived from normal saline by substituting K^+ for Na^+. In one experiment (synapse 10), high-K^+ saline contained 30 mM K^+. Zero-calcium saline was derived from low-Ca^{2+} saline modified by the omission of Ca^{2+} and the addition of 2 mM $MgCl_2$ and 2 mM EGTA. In an attempt to maximize vesicle depletion at stimulated synapses, some sacculi were incubated in high-K^+ saline on ice because cold has been reported to block endocytosis at photoreceptor ribbon synapses (Schaeffer and Raviola, 1978). For some conventional transmission electron microscopy (TEM) experiments, the temperatures were reversed. Tissue was then fixed in 3% glutaraldehyde in sodium cacodylate buffer (80 mM, with or without 4 mM $CaCl_2$) for 2–12 hr before decalcification in EDTA, postfixation in OsO_4, staining in uranyl acetate, and dehydration in ethanol as described in the basic protocol by Lenzi et al. (1999). Epithelia were then passaged through 100% ethanol, acetone, or propylene oxide before embedding in epon, araldite, or Spurr's (Spurr, 1969) resin. The osmosity of physiological salines was adjusted to 220–225 mM/Kg; the pH of salines and buffers was 7.23–7.25.

Sections for TEM and electron tomography were cut, stained, and imaged as described (Lenzi et al., 1999). For electron tomography, 0.5 μm sections were imaged at a magnification of 30,000×, and a series of 61 micrographs were acquired on film in 2° tilt-increments. Some data sets were obtained remotely using an updated version of the telemicroscopy system described previously (Lenzi et al., 1999).

Electron Tomography

We used electron tomography to reconstruct the 3D volume of the tissue section as described previously (Lenzi et al., 1999). Briefly, the negatives of the tilt series were digitized, aligned, and backprojected to generate a digital volume ranging in size from 342 × 282 × 78 to 600 × 400 × 123 voxels. Voxels were cubes, 2.7–2.9 nm on a side. The ultrastructure of the synapse could then be inspected by shuffling through the volume one plane (one voxel thick) at a time. Organelles and structures were manually traced in each *x-y* plane in which they appeared, before being surfaced and rendered. Six of the ten volumes (synapses 2, 3, 4, 9, 10, and 11) were acquired, reconstructed, traced, and analyzed blind.

Geometrical Analysis

TEM

All synapses in each tissue section were photographed, and two observers blind to the treatment counted the number of vesicles

within 30 nm of each SB. Micrographs were then digitized, and SB perimeters measured with NIH Image software. For each SB, the average count of the two observers was divided by the perimeter length and expressed as a percentage of the 1D maximum packing density of 40 nm diameter spheres (1D close-pack = 1 vesicle/40 nm of perimeter length).

Electron Tomography

We mapped the diameter and location of coated and synaptic vesicles by identifying the *x-y* plane of largest cross-section, tracing the vesicle perimeter along the middle of the membrane, and fitting a circle of area equal to the traced polygon. Vesicles were then rendered as spheres having the diameter and centers of the fitted circles (Lenzi et al., 1999). A vesicle was classified as SB associated if in the plane of its largest cross-section it was tethered to, or within 30 nm of the SB (Lenzi et al., 1999). A vesicle was classified as docked if no space could be seen between its membrane and the plasma membrane in at least one *x-y* plane. The plane of contact was sometimes different from the plane of largest cross-section (Lenzi et al., 1999).

A sphere was fit to each SB as described in (Lenzi et al., 1999). To calculate vesicle distributions around the synapse, we rotated and translated the (x, y, z) coordinates of the reconstruction such that the SB center was on the z axis and the presynaptic membrane coincided as closely as possible with the horizontal plane at $z = 0$, using a least-squares fitting procedure. The origin of this coordinate system was defined as the center of the active zone. To determine the density of docked vesicles as a function of distance from the active zone center, docked vesicle centers were projected onto the $z = 0$ plane and binned according to distance from the origin. The number of vesicles in each bin was divided by the plasmalemmal surface area in the bin to determine the average vesicle density. Docked vesicle densities were expressed as a fraction of the maximum number of 40 nm spheres that could be packed into a given area (2D close-pack = 1 vesicle/1386 nm^2). To calculate the density of nondocked vesicles as a function of distance from the SB center, we partitioned the cytoplasm into concentric spherical shells around the SB center, assigned each vesicle to a shell based on the position of its center, and divided the number of vesicles in each shell by the volume of reconstructed cytoplasm contained within that cell. Vesicle densities were expressed as a fraction of the maximum number of 40 nm spheres that could be packed into a given volume (3D close-pack = 1 vesicle/41,569 nm^3).

SB-associated vesicles were arrayed in a monolayer around the SB, with their centers located ~40 nm from the SB surface (20 nm vesicle radius + 20 nm tether length). To calculate the density of these vesicles as function of latitude on the SB, the center of each SB-associated vesicle was projected radially onto a sphere concentric with the SB having a radius 40 nm larger than the SB radius. The z axis coordinates of the projected vesicles were normalized to lie between 0 (the membrane pole) and 1 (the opposite pole) and grouped into ten bins, thus dividing the SB into ten bands of equal area. The number of vesicles in each band was divided by the area of the band contained within the reconstructed cytoplasm to determine the vesicle density, expressed as a fraction of 2D close-pack.

To calculate the density of outlying vesicles as a function of distance perpendicular to the membrane, vesicles were binned according to their z coordinate in the transformed coordinate system; to eliminate the effect of the space occupied by the SB, a 300 nm radius cylinder centered on the z axis was excluded from this calculation.

For calculating membrane concentrations, we considered the volume of available cytoplasm, consisting of the volume of the reconstruction minus the volumes of mitochondria, the SB, the postsynaptic cell, and extracellular space. Organelle volumes were calculated by summing the areas of profiles traced in each plane and multiplying by the voxel size (the plane thickness). Organelle areas were calculated by summing the perimeters traced in each plane and multiplying by the voxel size. Vesicle areas were calculated using the average vesicle diameter for each reconstruction, and assuming vesicles were spheres.

To estimate the expected frequency of random close encounters between vesicles and the plasmalemma that would be counted as "docked" by our criterion, we used the average vesicle concentration in the neighboring cytoplasm to calculate the number of vesicles that would lie within 10 nm of the plasma membrane. Because we could have resolved a 10 nm gap between a vesicle and the plasma membrane in most cases, these are overestimates.

Electrophysiology

Sacculi were dissected and furrowed as for electron microscopy, and superfused with normal saline on the stage of a fluorescence microscope. A microelectrode, normal to the apical surface of the hair cells, was inserted into the epithelium, and once a stable recording was achieved, the bath volume was exchanged with 45 mM K^+ saline. Microelectrodes had resistances of 220 MΩ after the shank was filled with 4% Lucifer Yellow (in H_2O) and the shaft backfilled with 0.5M LiCl. Junction potential changes were negligible between salines.

Acknowledgments

We thank Drs. Miriam Goodman, Brian Edmonds, and the late Stephen J. Young for much helpful discussion, Naoko Yamada for help with electron microscopy, and Martin Hadida-Hassan and Stephan Lamont for help with computing. Supported by NIH grants NS27142 to W.M.R. and NS36069 to M.H.E. The NIH National Center for Research Resources supports the National Center for Microscopy and Imaging Research through award RR04050 to M.H.E, which also contributed to this project.

Received: March 25,2002
Revised: August 14, 2002

References

Armstrong, C.E., and Roberts, W.M. (1998). Electrical properties of frog saccular hair cells: distortion by enzymatic dissociation. J. Neurosci. *18*, 2962–2973.

Beutner, D., Voets, T., Neher, E., and Moser, T. (2001). Calcium dependence of exocytosis and endocytosis at the cochlear inner hair cell afferent synapse. Neuron *29*, 681–690.

Brodin, L., Löw, P., and Shupliakov, O. (2000). Sequential steps in clathrin-mediated synaptic vesicle endocytosis. Curr. Opin. Neurobiol. *10*, 312–320.

Brunger, A.T. (2000). Structural insights into the molecular mechanism of Ca^{2+}-dependent exocytosis. Curr. Opin. Neurobiol. *10*, 293–302.

Bunt, A.H. (1971). Enzymatic digestion of synaptic ribbons in amphibian retinal photoreceptors. Brain Res. *25*, 571–577.

Furukawa, T., Kuno, M., and Matsuura, S. (1982). Quantal analysis of a decremental response at hair cell-afferent fibre synapses in the goldfish sacculus. J. Physiol. *322*, 181–195.

Gad, H., Löw, P., Zotova, E., Brodin, L., and Shupliakov, O. (1998). Dissociation between Ca^{2+}-triggered synaptic vesicle exocytosis and clathrin-mediated endocytosis at a central synapse. Neuron *21*, 607–616.

Glowatzki, E., and Fuchs, P.A. (2002). Transmitter release at the hair cell ribbon synapse. Nat. Neurosci. *5*, 147–154.

Gray, E.G., and Pease, H.L. (1971). On understanding the organisation of the retinal receptor synapse. Brain Res. *35*, 1–15.

Griesinger, C.B., Richards, C.D., and Ashmore, J.F. (2002). Fm1-43 reveals membrane recycling in adult inner hair cells of the mammalian cochlea. J. Neurosci. *22*, 3939–3952.

Hama, K., and Saito, K. (1977). Fine structure of the afferent synapse of the hair cells in the saccular macula of the goldfish, with special reference to the anastomosing tubules. J. Neurocytol. *6*, 361–373.

Harlow, M., Ress, D., Koster, A., Marshall, R.M., Schwarz, M., and McMahan, U.L. (1998). Dissection of active zones at the neuromuscular junction by EM tomography. J. Physiol. (Paris) *92*, 75–78.

Harlow, M.L., Ress, D., Stoschek, A., Marshall, R.M., and McMahan, U.L. (2001). The architecture of the active zone material at the frog's neuromuscular junction. Nature *409*, 479–484.

Heidelberger, R. (1998). Adenosine triphosphate and the late steps in

calcium-dependent exocytosis at a ribbon synapse. J. Gen. Physiol. *111*, 225–241.

Henry, W.R., and Mulroy, M.J. (1995). Afferent synaptic changes in auditory hair cells during noise-induced temporary threshold shift. Hear. Res. *84*, 81–90.

Heuser, J.E., and Reese, T.S. (1973). Evidence for recycling of synaptic vesicle membrane during transmitter release at the frog neuromuscular junction. J. Cell Biol. *57*, 315–344.

Hibino, H., Pironkova, O., Onwumere, O., Vologodskaia, M., Hudspeth, A.J., and Lesage, F. (2002). RIM binding proteins (RBPs) couple Rab3-interacting molecules (RIMs) to voltage-gated Ca^{2+} channels. Neuron *34*, 411–423.

Jacobs, R.A., and Hudspeth, A.J. (1990). Ultrastructural correlates of mechanoelectrical transduction in hair cells of the bullfrog's internal ear. Cold Spring Harb. Symp. Quant. Biol. *55*, 547–561.

Juusola, M., French, A.S., Uusitalo, R.O., and Weckström, M. (1996). Information processing by graded-potential transmission through tonically active synapses. Trends Neurosci. *19*, 292–297.

Kollmar, R., Fak, J., Montgomery, L.G., and Hudspeth, A.J. (1997a). Hair cell-specific splicing of mRNA for the α1D subunit of voltage-gated Ca^{2+} channels in the chicken's cochlea. Proc. Natl. Acad. Sci. USA *94*, 14889–14893.

Kollmar, R., Montgomery, L.G., Fak, J., Henry, L.J., and Hudspeth, A.J. (1997b). Predominance of the α1D subunit in L-type voltage-gated Ca^{2+} channels of hair cells in the chicken's cochlea. Proc. Natl. Acad. Sci. USA *94*, 14883–14888.

Koschak, A., Reimer, D., Huber, I., Grabner, M., Glossmann, H., Engel, J., and Striessnig, J. (2001). α1D (Cav1.3) subunits can form L-type Ca^{2+} channels activating at negative voltages. J. Biol. Chem. *276*, 22100–22106.

Lagnado, L., Gomis, A., and Job, C. (1996). Continuous vesicle cycling in the synaptic terminal of retinal bipolar cells. Neuron *17*, 957–967.

Leenders, A.G., Scholten, G., de Lange, R.P., Lopes da Silva, F.H., and Ghijsen, W.E. (2002). Sequential changes in synaptic vesicle pools and endosome-like organelles during depolarization near the active zone of central nerve terminals. Neuroscience *109*, 195–206.

Lenzi, D., and von Gersdorff, H. (2001). Structure suggests function: the case for synaptic ribbons as exocytotic nanomachines. Bioessays *23*, 831–840.

Lenzi, D., Runyeon, J.W., Crum, J., Ellisman, M.H., and Roberts, W.M. (1999). Synaptic vesicle populations in saccular hair cells reconstructed by electron tomography. J. Neurosci. *19*, 119–132.

Li, J.L., and Schwarz, T. (1999). Genetic evidence for an equilibrium between docked and undocked vesicles. Philos. Trans. R. Soc. Lond. B. Biol. Sci. *354*, 299–306.

Matsubara, A., Laake, J.H., Davanger, S., Usami, S., and Ottersen, O.P. (1999). Organization of AMPA receptor subunits at a glutamate synapse: a quantitative immunogold analysis of hair cell synapses in the rat organ of Corti. J. Neurosci. *16*, 4457–4467.

Mennerick, S., and Matthews, G. (1996). Ultrafast exocytosis elicited by calcium currents in synaptic terminals or retinal bipolar neurons. Neuron *17*, 1241–1249.

Morgans, C.W. (2000). Neurotransmitter release at ribbon synapses in the retina. Immunol. Cell Biol. *78*, 442–446.

Moser, T., and Beutner, D. (2000). Kinetics of exocytosis and endocytosis at the cochlear inner hair cell afferent synapse of the mouse. Proc. Natl. Acad. Sci. USA *97*, 883–888.

Mulroy, M.J., Fromm, R.F., and Curtis, S. (1990). Changes in the synaptic region of auditory hair cells during noise-induced temporary threshold shifts. Hear. Res. *49*, 79–88.

Muresan, V., Lyass, A., and Schnapp, B.J. (1999). The kinesin motor KIF3A is a component of the presynaptic ribbon in vertebrate photoreceptors. J. Neurosci. *19*, 1027–1037.

Murthy, V.N., and Stevens, C.F. (1999). Reversal of synaptic vesicle docking at central synapses. Nat. Neurosci. *2*, 503–507.

Nadol, J.B. (1990). Synaptic morphology of inner and outer hair cells of the human organ of Corti. J. Electron Microsc. Tech. *15*, 187–196.

Parsons, T.D., Lenzi, D., Almers, W., and Roberts, W.M. (1994). Calcium-triggered exocytosis and endocytosis in an isolated presynaptic cell: capacitance measurements in saccular hair cells. Neuron *13*, 875–883.

Richards, D.A., Guatimosim, C., and Betz, W.J. (2000). Two endocytic recycling routes selectively fill two vesicle pools in frog motor nerve terminals. Neuron *27*, 551–559.

Roberts, W.M. (1994). Localization of calcium channels by a mobile calcium buffer in frog saccular hair cells. J. Neurosci. *14*, 3246–3262.

Roberts, W.M., Jacobs, R.A., and Hudspeth, A.J. (1990). Colocalization of ion channels involved in frequency selectivity and synaptic transmission at presynaptic active zones of hair cells. J. Neurosci. *10*, 3664–3684.

Rouze, N.C., and Schwartz, E.A. (1998). Continuous and transient vesicle cycling at a ribbon synapse. J. Neurosci. *18*, 8614–8624.

Schacher, S.M., Holtzman, E., and Hood, D.C. (1974). Uptake of horseradish peroxidase by frog photoreceptor synapses in the dark and the light. Nature *249*, 261–263.

Schacher, S.M., Holtzman, E., and Hood, D.C. (1976). Synaptic activity of frog retinal photoreceptors –a peroxidase uptake study. J. Cell Biol. *70*, 178–192.

Schaeffer, S.F., and Raviola, E. (1978). Membrane recycling in the cone cell endings of the turtle retina. J. Cell Biol. *79*, 802–825.

Schikorski, T., and Stevens, C.F. (1997). Quantitative ultrastructural analysis of hippocampal excitatory synapses. J. Neurosci. *17*, 5858–5867.

Schmitz, F., Bechmann, M., and Drenckhahn, D. (1996). Purification of synaptic ribbons, structural components of the photoreceptor active zone complex. J. Neurosci. *16*, 7109–7116.

Schmitz, F., Königstorfer, A., and Südhof, T.C. (2000). RIBEYE, a component of synaptic ribbons: a protein's journey through evolution provides insight into synaptic ribbon function. Neuron *28*, 857–872.

Siegel, J.H., and Brownell, W.E. (1986). Synaptic and golgi membrane recycling in cochlear hair cells. J. Neurocytol. *15*, 311–328.

Spassova, M., Eisen, M.D., Saunders, J.C., and Parsons, T.D. (2001). Chick cochlear hair cell exocytosis mediated by dihydropyridine-sensitive calcium channels. J. Physiol. *535*, 689–696.

Spurr, A.R. (1969). A low-viscosity epoxy embedding medium for electron microscopy. J. Ultrastruct. Res. *26*, 31–43.

Stevens, C.F., and Tsujimoto, T. (1995). Estimates for the pool size of releasable quanta at a single synapse for the time required to refill the pool. Proc. Natl. Acad. Sci. USA *92*, 846–849.

Vollrath, L., and Spiwoks-Becker, I. (1996). Plasticity of retinal ribbon synapses. Microsc. Res. Tech. *35*, 472–487.

von Gersdorff, H., and Matthews, G. (1994). Dynamics of synaptic vesicle fusion and membrane retrieval in synaptic terminals. Nature *367*, 735–739.

von Gersdorff, H., and Matthews, G. (1997). Depletion and replenishment of vesicle pools at a ribbon-type synaptic terminal. J. Neurosci. *17*, 1919–1927.

von Gersdorff, H., Vardi, E., Matthews, G., and Sterling, P. (1996). Evidence that vesicles on the synaptic ribbon or retinal bipolar neurons can be rapidly released. Neuron *16*, 1221–1227.

von Gersdorff, H., Sakaba, T., Berglund, K., and Tachibana, M. (1998). Submillisecond kinetics of glutamate release from a sensory synapse. Neuron *21*, 1177–1188.

Wagner, H.J. (1997). Presynaptic bodies ("ribbons"): from ultrastructural observations to molecular perspectives. Cell Tissue Res. *287*, 435–446.

Zenisek, D., Steyer, J.A., and Almers, W. (2000). Transport, capture and exocytosis of single synaptic vesicles at active zones. Nature *406*, 849–854.

Zucca, G., Bota, L., Milesi, V., Dagani, F., and Valli, P. (1992). Evidence for L-glutamate release in frog vestibular organs. Hear. Res. *63*, 52–56.